IEEE Photonics Journal
An IEEE Photonics Society Publication

# High-Resolution Spectrometer-on-Chip Based on Digital Planar Holography

Volume 3, Number 5, October 2011

Christophe Peroz
Alexander Goltsov
Scott Dhuey
Pavel Sasorov
Bruce Harteneck
Igor Ivonin
Sergey Kopyatev
Stefano Cabrini
Sergey Babin
Vladimir Yankov

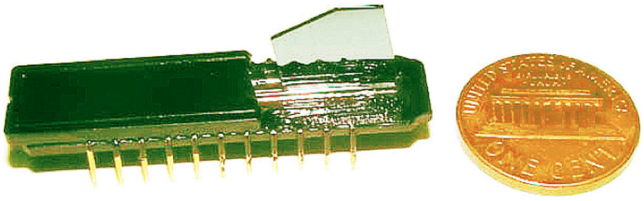

DOI: 10.1109/JPHOT.2011.2168950
1943-0655/$26.00 ©2011 IEEE

IEEE photonics SOCIETY

IEEE

# High-Resolution Spectrometer-on-Chip Based on Digital Planar Holography

**Christophe Peroz,[1] Alexander Goltsov,[2] Scott Dhuey,[3] Pavel Sasorov,[2] Bruce Harteneck,[3] Igor Ivonin,[2] Sergey Kopyatev,[2] Stefano Cabrini,[3] Sergey Babin,[1] and Vladimir Yankov[2]**

[1]aBeam Technologies, Castro Valley, CA 94546 USA
[2]Nano-Optic Devices, Santa Clara, CA 95054 USA
[3]The Molecular Foundry, LBNL, Berkeley, CA 94702 USA

*DOI: 10.1109/JPHOT.2011.2168950*
*1943-0655/$26.00 ©2011 IEEE*

Manuscript received September 8, 2011; accepted September 13, 2011. Date of publication September 29, 2011; date of current version October 4, 2011. The work done at the Molecular Foundry was supported by the Office of Science, Office of Basic Energy Sciences, of the U.S. Department of Energy under Contract DE-AC02-05CH11231. Corresponding author: C. Peroz (e-mail: cp@abeamtech.com).

**Abstract:** Digital planar holography enables the creation of a new generation of integrated photonic circuits with desired transfer function. We give here, for the first time, the basis for designing computer-generated planar holograms and demonstrate their application for spectroscopy-on-chip. Nanospectrometer chips are demonstrated with unmatched spectral resolution of up to $2 \cdot 10^5$. A specific configuration is demonstrated for easy integration of planar holograms into the full spectrometer system. The ultraminiaturization and very high performances of the devices are a breakthrough in spectroscopy and open a novel route for the digital processing of light.

**Index Terms:** Holography, nanofabrication, spectrometer.

## 1. Introduction

Holography is a powerful method for encoding any optical information such as an image or any transmission function into a material substrate [1]. A hologram typically consists of a combination of millions of subwavelength features recorded on a transparent media. The first analog holograms were made with conventional photomaterials, copying existing objects only [1]. Computer-generated holography emerged when lithography processes moved to subwavelength patterning [2]. Computer program generates the position of millions of holographic pixels, which are replicated onto a mask or film. Until very recently, computer-generated holography was mostly limited to reproducing small pictures like logos [3]. The development of holographic based photonic devices is difficult in the case of 3-D thick holograms where the light travels through a hologram in a very short pathway. To scatter light on micrometer scale, the perturbations must be strong, thus leading to ghost images, loss of light, and limited capacity to write many images on the same hologram [4], [5]. The utilization of planar waveguides in holography for the first time was proposed in 1976 [6]. Since then, a number of approaches have been studied to develop in-plane [7] and off-plane [8], [9] computer-generated holograms based on planar waveguides. The idea of our new planar geometry named digital planar holography (DPH) is to let the light travel inside a hologram for thousands of wavelengths $(\lambda)$ in order to increase significantly the possibility for light processing. This concept was used for volume holographic memory [4], but the development of computer-generated volume holograms is very limited due to their difficult and expensive fabrication [10]. As opposed to this, the DPH technology allows easy writing of an arbitrary computer-generated hologram onto a planar

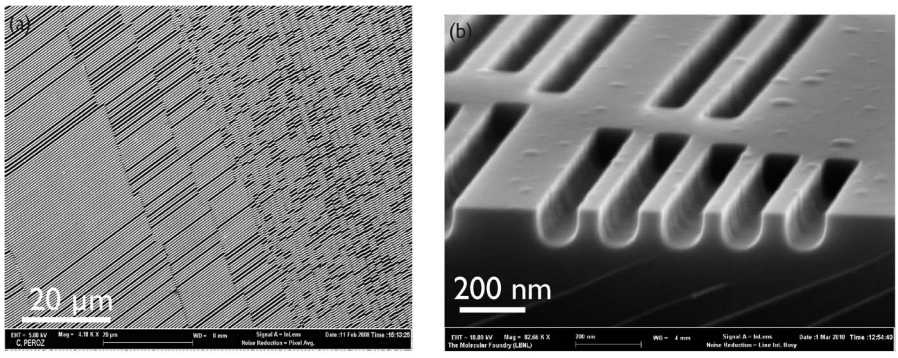


Fig. 1. Scanning electron microscope pictures of a computer-generated hologram. (a) Top view and (b) cross section of a hologram etched into silica waveguide core. The linewidth of etched dashes is around 100 nm.

waveguide with very long light pathway [11], [12]. We apply here this approach for creating and reproducing photonic transfer functions of very high-resolution spectrometer-on-chip.

Photospectrometers are standard tools for analyzing the spectral content of light and are used in various fields from biomedicine to materials sciences. The core-component of spectrometers is a dispersive element that deflects the light according to its wavelength $(\lambda)$. All known commercial spectrometers are based on old-fashioned optical elements such as Bragg gratings, or prisms, for which the light is deflected continuously in its full desired range of wavelengths. The optical elements are mechanically tuned according to the wavelength to be detected. High-resolution spectrometers are mainly limited to expensive and bulky systems [13], whereas the microelectromechanical systems (MEMS)-based spectrometers [14]–[16] are still complex and expensive systems which are not suitable for full-chip integration, and their performance is still limited in terms of spectral resolution. Arrayed waveguide grating spectrometers [17] have recently emerged as a promising alternative and can reach spectral resolution of around 0.2 nm in the visible range [18], but the technology is not very versatile, and crosstalk between channels is still large.

The integration of the optical spectrometer into compact and high sensitive detection systems, as laboratory-on-chip devices, has been held up by the inadequacy between integration requirements and properties of actual dispersive elements. Recent progress in nanophotonics allows the control of the light at the nanometer scale and promises the emergence of ultraminiaturized spectrometers based on photonic crystals [19], [20], arrayed waveguide gratings [21], or microring resonators [22]. However, these approaches are not versatile, and the actual spectrometer chips are limited to a small number of channels and near-infrared wavelength range. In general terms, a spectrometer is characterized by Fourier components

$$f_{in}(x, y, \omega) \quad \text{and} \quad f_{out}(x, y, \omega) \tag{1}$$

of incoming $(f_{in})$ and outgoing $(f_{out})$ electric field components of the waves propagating between input and detector array. These functions are directly related to the variation of the effective refractive index $\Delta \boldsymbol{n}$ in the following form:

$$\Delta n(x, y) = \int f_{in}(x, y, \omega) f_{out}(x, y, \omega)\, d\omega. \tag{2}$$

Our simple idea consists of converting the transfer function $\Delta n$ of desired spectrometer properties to a binary form and of replicating this function into 2-D computer-generated holograms.

A computer-generated hologram consists of millions of lines (pixels) etched into a planar waveguide core (see Fig. 1). The position of each line represents one "bit" (0 or 1) of the hologram, and each bit influences the whole transfer function of the photonic element. The linewidth (w) of the dashes composing the hologram is defined by the operating wavelength and is usually close to one quarter of the guided light wavelength $(\lambda)$, resulting in strong backscattering. For spectrometers

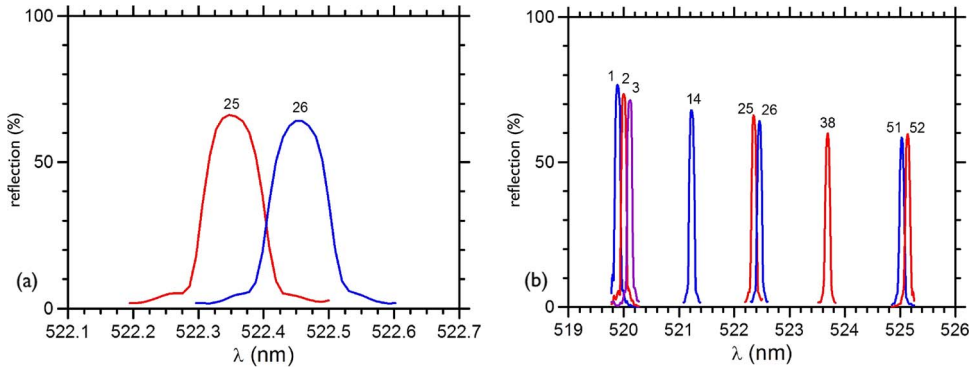


Fig. 2. Simulation of dispersion curve for one nanospectrometer. Simulated response function for one 52-channel spectrometer for (a) two adjacent 25 and 26 channels and (b) for channels 1, 2, 3, 14, 25, 26, 35, 51, and 52.

with oblique reflections (see Fig. 2), the linewidth is larger and is determined by the angle between incoming and outgoing beams. The depth of lines depends on the refractive index contrast between the waveguide core and the upper cladding. The total number of lines defines the spectral selectivity and the number of channels. The concept of our spectrometer-on-chip is based on the simple multiplexer/demultiplexer-on-chip devices proposed by Henry *et al.* [23]. Their component consisted from four separate elliptical Bragg gratings, each focusing (property of ellipse) light of specific wavelength (property of grating period). Since the gratings should be placed in a row, a 100-channel device would be by far too long. In our DPH configuration, all channels are written on the same surface, and the hologram has the same length, as a single channel device, based on the elliptical Bragg grating. The photonic bandgap concept is useful to explain the flat top of a transfer function [24]. Light waves cannot propagate in the bandgap; therefore, in an ideal model, all energy will be reflected in the same direction. The width $\Delta\omega$ of the bandgap is proportional to the variation $\Delta n$ of effective refractive index of the corresponding Fourier harmonic with a typical variation: $\Delta\omega/\omega = \Delta n/n$. Inside the bandgap, the amplitude of light decays exponentially with characteristic length L, which is also close to the length of our holograms

$$L = \lambda n/\Delta n \approx 10^3 - 10^4\lambda. \tag{3}$$

## 2. Digital Planar Holography

We have developed a specific [25] numerical code—called Program SPECTROPLAN—in order to generate e-drawings of our planar holograms. The method allows the design of a large variety of device geometries—direct input, angular input, and custom-made spectral holograms with discrete dispersion. Our numerical code allows finding the Green function of the stationary wave equation for the monochromatic light propagating along a planar hologram, as an element of the optical design. The boundary conditions are the source at the place of input fiber tip and outgoing waves from the hologram. The program finds all transverse electric (TE) and transverse magnetic (TM) core modes, which can propagate both in the planar wafer and near in outer space. The hologram is modeled by the binary variation of the effective refraction index $\Delta n$ for a particular mode due to the depth of the dashes. Mathematically, the Green function of the particular equation can be expressed as the solution of an integral equation. In general, this equation can only be solved by iterations. The first iteration is known as the first perturbation or one scattering solution. Multiple reflections from the hologram structure require multiple iterations. Each iteration is expensive computationally since it requires the integration over the hologram surface. No existing code can quickly perform such computations, except for a simple combination of regular Bragg subgratings of macroscopic size. Another available technique, i.e., the relaxation method, is also ineffective computationally, since

the ratio of the hologram size to the size of the feature can be as large as 1 cm/100 nm $= 10^5$, and thus, many time steps are required until relaxation. Our code is fast and efficient since it can fully solve the problem by integration over the hologram surface. We solve a specific problem of binary hologram, and only matching the boundary conditions at the surface of the hologram features is required.

The approach is similar to the finite element method (FEM), except that the number of the elements can be as large as 1 billion, which makes FEM inefficient. We settle this inefficiency by using small parameters in our problem. In particular, we use low variation of the refraction index in our holograms. This approximation is valid because the etch depth of dashes is usually quite small in comparison with the core thickness, which makes the useful induced scattering much stronger than the light scattering. SPECTROPLAN-code is used for the generation of elementary binary DPH structures describing the transfer function of one spectrometer. First, we calculate a continuous generation function in which the interference of incoming and outgoing waves from the desired spatial locations is taken with some initial weights and phases. Then, the generation function is digitalized—the positive values of the function are reserved for the etched areas. After that, we represent (with the desired accuracy) the etched areas by the rectangular of the same width. Then we apply rarefaction to reduce duty ratio and make the printing stable by reducing the proximity effects. Finally, we apply additional rarefaction at the ends of the hologram (spatial apodization) to reduce the light intensity in the sidelobes of radiation. The direction angle of incoming and outgoing waves in the DPH needs to be kept low enough in order to reduce existing transient effects at both sides of the hologram, where the input and output beams do not overlap, limiting the efficiency of induced reflection.

A computer-generated planar hologram is generated as a synthetic composition of $N$ gratings, where $N$ is the number of channels of DPH-device. Each subgrating is formed by a system of ellipses with the same focus. One focus is placed at the input point of the DHP, which is common for all channels, whereas the second focus is placed at the output point of the channel. The position of the output point depends on the channel number. Usually, the output points are positioned equidistantly along an output line of the DHP. The amplitude of reflection of a wave on a single dash is proportional to $\Delta n/n$. If total reflection is small, then its amplitude is proportional to

$$M\frac{\Delta n}{n} \propto L\frac{\Delta n}{n} \tag{4}$$

where $M$ is total number of dashes along the input beam. The intensity of the reflection is proportional to square of $L$ and square of $\Delta n/n$. Thus, to reflect about half of the input beam, the following scaling should be fulfilled:

$$1 = C_1\frac{\Delta n}{n}kL \tag{5}$$

where $k$ is a typical wavenumber of the input wave, and $C_1$ is some numerical coefficient that is rather small ($\sim$0.05), determined by simulations with our software SPECTROPLAN, and depends on general geometry of the DHP and number of channels.

The second important scaling is determined by

$$\delta kl = C_2 \tag{6}$$

where $\delta k$ is width of the spectral response function of each channel.

The spectral channel spacing $\Delta k$ and the width $\delta k$ of the channels are related as

$$\Delta k = C_3\delta k. \tag{7}$$

Computer experiments with the code SPECTROPLAN show that the coefficients $C_2$ and $C_3$ are on the order of 1, depending on the entire geometry of the DPH and belong the interval 0.5–1. The interval of spectral space between the wave vectors of marginal channels of DPH is denoted as $Dk$. The total number of channels N and the length of holograms $L$ are finally determined with the (5)–(7).

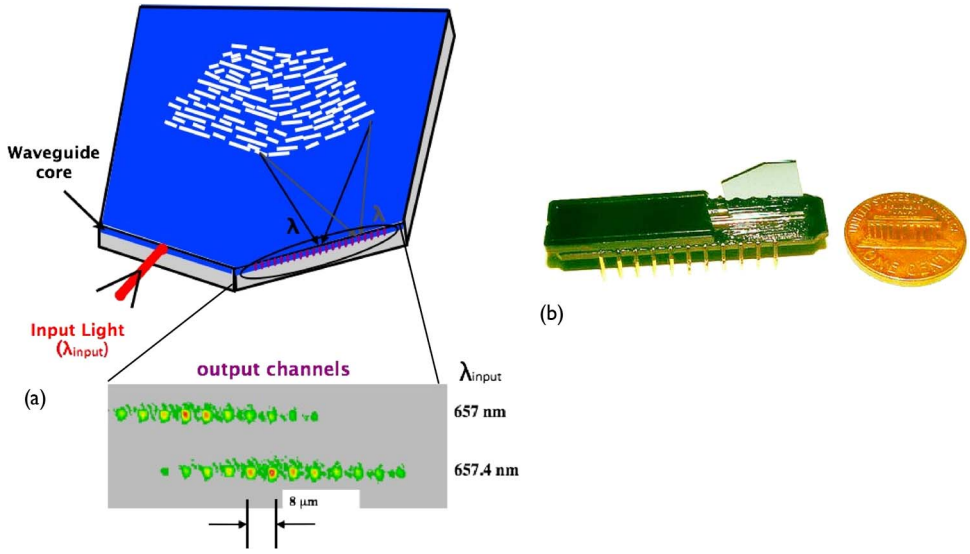


Fig. 3. Nanospectrometer with computer-generated hologram. (a) Schematical view of a DPH spectrometer with angular input light. The diffracted light is focused in some specific output channels according to the input wavelength value. (b) Optical picture of a DPH chip coupled with a CCD array.

An example of results for simulations of wave propagation with SPECTROPLAN is depicted in Fig. 2. A 52-channel spectrometer in a spectral range of 520–525 nm has been computed with a core-cladding refractive index contrast of 3%. Details on the spectral response function of two adjacent channels [see Fig. 2(a)], as well as for various channels along the spectral range [see Fig. 2(b)], demonstrate that the peak reflections are almost uniform over the whole spectral range.

## 3. Experimental Details and Results

Holograms were fabricated into a $SiO_2Ge_x$ waveguide core by electron beam lithography and reactive ion etching. Spectrometer chips are measured with a homemade optical setup [26], [27]. Two laser sources were used to tune wavelengths between 400 and 700 nm. Details on nanofabrication of holograms and optical characterization of spectrometer chips are given in [26] and [27]. Two families of DPH Spectroscopes have been fabricated and tested: the devices with direct input–output of light as reported in [24] and a new configuration with angular input of light facilitating the DPH-detector assembly (see Fig. 3). Light is coupled to the device via single mode fiber, the output of which is either butt coupled to the hologram input or focused to the input with a micro objective. Depending on the hologram design, the required alignment accuracy is about 0.5 $\mu$m in the fast (i.e., perpendicular to the planar waveguide with the hologram) direction and 3–5 $\mu$m in the slow direction along the output edge of the planar. A linear CCD array is attached in a close proximity to the device output plane. Special attention was paid to get information required for optimizing the design of spectroscopes and for finding optimum conditions in fabrication process in order to maximize the reflection efficiency of the device while keeping low crosstalk between channels.

Nanospectrometers with a broad range of parameters have been successfully demonstrated (Figs. 4 and 5). The number of channels is varied from 22 up to 1000, the channel pitch—from 1 to 50 $\mu$m and the channel spacing—from 1 nm to 0.015 nm. As an example, Fig. 4 displays the spectrum of a tunable testing laser (around 0.3 nm full-width at half-maximum value) measured at the output of a 64-channel spectroscope. It clearly demonstrates the discrete character of dispersion in digital holographic spectrometers. The channel spacing for this device is around 0.015 nm, while the spectral width of the channel is around 0.005 nm, corresponding to a spectral resolution $(\Delta\lambda/\lambda)$ higher than 1.2 $10^5$. In general, the spectral resolution of DPH spectrometers is limited by the length of its hologram and the properties of the planar waveguide core films. The spectral resolution is directly proportional to the numbers of dashes for one hologram. A resolution around $10^5$ is close to the

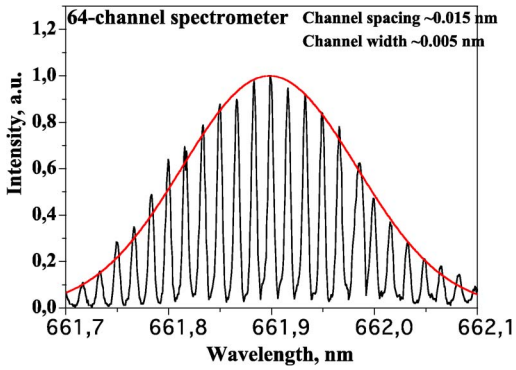


Fig. 4. Optical Spectroscopic Measurements. Response of a 64-channel DPH spectroscope to a probe laser of 0.3-nm FWHM bandwidth. The channel spacing is around 0.015 nm, and the channel width of detection is around 0.005 nm, corresponding to a spectral selectivity of around 1.3 $10^5$.

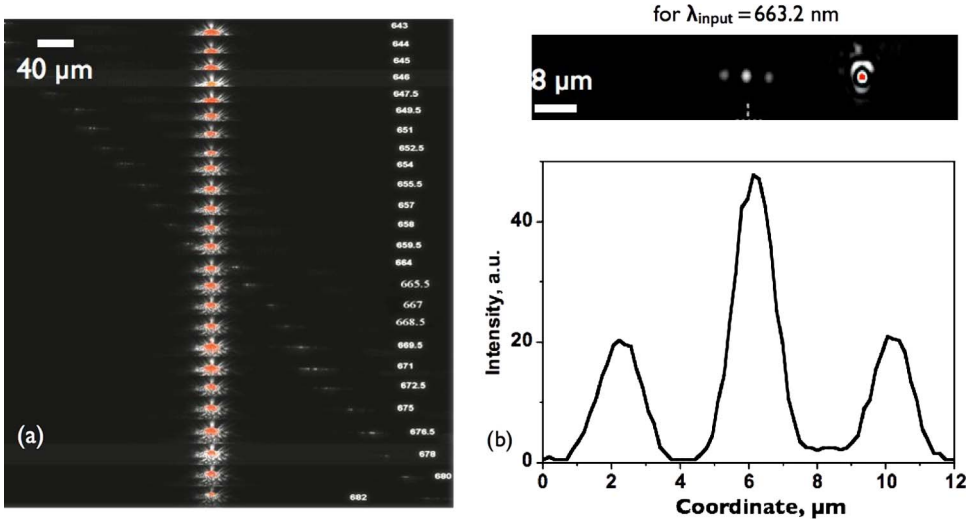


Fig. 5. (a) Successive images of the input–output plane of a 128-channel device for different wavelength (TE mode), where the central bright spot corresponds to the input beam. The input wavelength increases from 643 nm (top slide) to 682 nm (bottom slide) with a constant increment of 0.5 nm. (b) Detail on the intensity distribution at the input-output edge for same device than in (b), where the spacing between each output channel is 4 $\mu$m.

maximum possible with present technologies for wafer fabrication (optical homogeneity) and lithography as well.

The optical characteristics of fabricated photospectrometer were measured, such as channel spacing, channel pitch, spectral dispersion, and the shape of channels in spectral space. To illustrate this, the responses taken at the output of a 128-channel silica-on-silicon DPH spectrometer to a probe laser for various input wavelength values are depicted in Fig. 5(a). The pronounced crosstalk observed in the response curve cannot be accounted for only by the finite width of a probe laser but is also a specific feature of this given device, which is in full accord with simulation. To retain spectral lines when interpreting the spectroscopic measurement, the spectroscopes with discrete dispersion were designed to have the crosstalk of 10%–30%. The close values of a crosstalk were observed in experiments.

The radiation scattered out from a hologram in the direction perpendicular to the DPH surface was also studied to measure the performance of holograms. In our early experiments, it was shown that the fraction of light, scattered in 3-D, does not exceed 2–3% for 4-channel devices but increases by a factor of 2 to 3 following the increase in the number of channels up to 16 [12]. It corresponds to

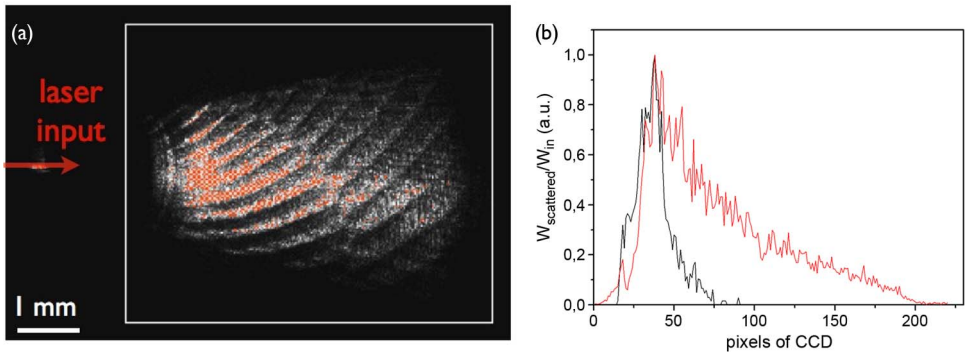


Fig. 6. Energy distribution over the computer-generated hologram at 659-nm wavelength. (a) Top view of the 128-channel hologram illuminated with testing laser beam. Bright red color in the image corresponds to higher intensity of scattered light. (b) Propagation of the light along the horizontal direction for depth dashes of 120 nm (red) and 250 nm (black).

TABLE 1

Dissipation energy on holograms ratio of energy for light scattered ($W_{scattered}$) at the surface of one hologram normalized to the input power ($W_{in}$). The values of $W_{scattered}$ and $W_{in}$ are integrated over the full surface of one hologram [see Fig. 4(a)]

| input wavelength (nm) | 532 | 655 | 656.4 | 657.6 | 659.3 |
|---|---|---|---|---|---|
| $W_{scattered}/W_{in}$ (a.u) for depth ~ 120 nm | 0.56 | 1.51 | 3.04 | 7.38 | 3.45 |
| $W_{scattered}/W_{in}$ (a.u) for depth ~ 250 nm | 0.94 | 1.59 | 1.66 | 0.44 | 0.51 |

energy losses in DPH multichannel devices and potentially decreases the spectrometer throughput. As first approximation, the intensity of scattered light is proportional to the local energy density in a hologram and reveals hologram performance. Different mechanisms contribute to the energy distribution of scattered light, namely, passive losses (volume absorption), back reflection of the light for resonant wavelengths, and upward scattering off the holograms. Fig. 6(a) shows an example of energy distribution taken in experiments with two 128-channel devices with direct input–output planes similar to that mentioned above. Resonant reflection band of holograms spans from 640 nm to 690 nm. The only difference between the two devices was the etching depth of the hologram grooves that is reflection efficiency. The increase in depth of dashes from 120 nm to 250 nm results in a sharper energy distribution close to the hologram's input [see Fig. 6(b)]. According to our estimates, the level of passive losses is negligible. Dissipation effects are mainly governed by 3-D scattering and resonant backward reflection in planar modes. Comparison of the fraction of scattered power for different input wavelengths is listed in Table 1. It is found that 3-D scattering is strongly affected by different spatial distribution of light energy along the planar hologram associated with different etching depths of the hologram. Fig. 6 shows that smaller etching depth increases the overall 3-D scattering, whereas the maximum relative flux per unit area does not vary with the depth. It is also observed that the maximum of the power-scattered perpendicular to the DPH is reached in the middle of the bandwidth of the spectrometer. The scattering power decreases toward the boundaries of the wavelength band and becomes minimal out off it, indicating that the energy of the light coupled in the planar core is mainly scattered upon the holograms. The measurement of the 3-D scattering is a useful tool for the

investigation of light propagation along the holograms. The spatial distribution of the scattered light gives information on the penetration of the beam. In this work, the scattered light is found to be a minor part of the total energy coupled into the planar. The strong correlation between the 3-D scattered power and the wavelength relative to resonant band, the number of channels, the depth etching, and the length of the hologram indicates clearly that this effect would not affect the desirable reflection of light in planar.

## 4. Conclusion

This paper demonstrates the highest performances for spectrometer-on-chip reported in the literature by computer-generated holograms and presents the distribution of the light in the holograms according to their etching depths. The basis of SPECTROPLAN software for fast designing planar holograms corresponding to a specific transfer function is presented. The method is successfully applied to fabricate nanospectrometer chips with unmatched spectral resolution up to $2.10^5$. We strongly believe that the full integration of computer-generated planar holograms at the level of one chip opens a route for development of miniaturized and very sensitive sensor-on-chip and is a powerful approach for the digital processing of light.

## Acknowledgment

The authors would like to thank E. Wood for technical assistance.

## References

[1] U. Schnars and W. Jueptner, *Digital Holography; Digital Hologram Recording, Numerical Reconstruction, and Related Techniques*. New York: Springer-Verlag, 2005.
[2] A. W. Lohmann and D. P. Paris, "Binary Fraunhoffer holograms, generated by computer," *Appl. Opt.*, vol. 6, no. 10, pp. 1739–1748, Oct. 1967.
[3] A. Rhody and F. Ross, *Holography Marketplace,* 8th ed. Scottsdale, AZ: Ross, 1999.
[4] J. F. Heanue, M. C. Bashaw, and L. Hesselink, "Volume holographic storage and retrieval of digital data," *Science*, vol. 265, no. 5173, pp. 749–752, Aug. 1994.
[5] H. J. Coufal, D. Psaltis, and G. T. Sincerbox, Eds., *Holographic Data Storage*. New York: Springer-Verlag, 2000.
[6] T. Suhara, H. Nishihara, and J. Koyama, "Waveguide holograms: A new approach to hologram integration," *Opt. Commun.*, vol. 19, no. 3, pp. 353–358, Dec. 1976.
[7] J. Saarinen, J. Turunen, and J. Huttunen, "Volume diffraction effects in computer-generated guided-wave holography," *Appl. Opt.*, vol. 33, no. 6, pp. 1035–1043, Feb. 1994.
[8] M. Li, S. Kristjansson, N. Eriksson, and A. Larsson, "Multiplexed computer-generated waveguide hologram using gratings with different spatial frequencies," *IEEE Photon. Technol. Lett.*, vol. 8, no. 12, pp. 1653–1655, Dec. 1996.
[9] T. Liao, S. Sheard, and G. Ya, "Demonstration of guided-wave optical fan-out using waveguide diffractive optical system," *Opt. Commun.*, vol. 137, no. 1–3, pp. 1–5, Feb. 1997.
[10] W. Cai, T. J. Reber, and R. Piestun, "Computer-generated volume holograms fabricated by femtosecond laser micromachining," *Opt. Lett.*, vol. 31, no. 12, pp. 1836–1838, Jun. 2006.
[11] V. Yankov, "Method of manufacturing an optical integrated nanospectrometer," U.S. Patent 12/806 361, Jan. 6, 2011.
[12] V. Yankov, S. Babin, I. Ivonin, A. Goltsov, A. Morozov, L. Polonskiy, M. Spector, A. Talapov, E.-B. Kley, and H. Schmidt, "Multiwavelength Bragg gratings and their application to optical MUX/DEMUX devices," *IEEE Photon. Technol. Lett.*, vol. 15, no. 3, pp. 410–412, Mar. 2003.
[13] N. Savage, "Spectrometers," *Nat. Photon.*, vol. 3, no. 10, pp. 601–602, Oct. 2009.
[14] V. Jovanov, J. Ivanchev, and D. Knipp, "Standing wave spectrometer," *Opt. Exp.*, vol. 18, no. 2, pp. 426–438, Jan. 2010.
[15] M. Kraft, A. Kenda, T. Sandner, and H. Schenk, "MEMS-based compact FT-spectrometers—A platform for spectroscopic mid-infrared sensors," in *Proc. IEEE Sens. Conf.*, 2008, pp. 130–133.
[16] T. Russin, M. Fralick, M. Kerber, A. Wang, and R. Waters, "Development of a MEMS-based Raman spectrometer," in *Proc. IEEE Sens. Conf.*, 2010, pp. 56–60.
[17] P. Cheben, J. H. Schmid, A. Delâge, A. Densmore, S. Janz, B. Lamontagne, J. Lapointe, E. Post, P. Waldron, and D.-X. Xu, "A high-resolution silicon-on-insulator arrayed waveguide grating microspectrometer with sub-micrometer aperture waveguides," *Opt. Exp.*, vol. 15, no. 5, pp. 2299–2306, Mar. 2007.
[18] N. Ismail, A. C. Baclig, P. J. Caspers, F. Sun, K. Wörhoff, R. M. de Ridder, M. Pollnau, and A. Driessen, "Design of low-loss arrayed waveguide gratings for applications in integrated Raman spectroscopy," in *Proc. CLEO*, 2010, pp. 1–2.
[19] B. Momeni, M. Chamanzar, E. Shah Hosseini, M. Askari, M. Soltani, and A. Adibi, "Strong angular dispersion using higher bands of planar silicon photonic crystals," *Opt. Exp.*, vol. 16, no. 18, pp. 14 213–14 220, Sep. 2008.
[20] B. Momeni, E. S. Hosseini, M. Askari, M. Soltani, and A. Adibi, "Integrated photonic crystal spectrometers for sensing applications," *Opt. Commun.*, vol. 282, no. 15, pp. 3168–3171, Aug. 2009.

[21] V. D. Nguyen, B. I. Akca, K. Wörhoff, R. M. de Ridder, M. Pollnau, T. G. van Leeuwen, and J. Kalkman, "Spectral domain optical coherence tomography imaging with an integrated optics spectrometer," *Opt. Lett.*, vol. 36, no. 7, pp. 1293–1295, Apr. 2011.
[22] B. B. C. Kyotoku, L. Chen, and M. Lipson, "Sub-nm resolution cavity enhanced microspectrometer," *Opt. Exp.*, vol. 18, no. 1, pp. 102–107, Jan. 2010.
[23] C. H. Henry, R. F. Kazarinov, Y. Shani, R. C. Kistler, V. Pol, and K. J. Orlovsky, "Four-channel wavelength division multiplexers and bandpass filters based on elliptical Bragg reflectors," *J. Lightw. Technol.*, vol. 8, no. 5, pp. 748–755, May 1990.
[24] E. Yablonovich, "Inhibited spontaneous emission in solid-state physics and electronics," *Phys. Rev. Lett.*, vol. 58, no. 20, pp. 2059–2062, May 1987.
[25] V. Yankov, "Method of digitally processing optical waves and an integrated planar optical device based on digital planar holography," U.S. Patent 20 090 190 195, Jul. 30, 2009.
[26] S. Babin, A. Bugrov, S. Cabrini, S. Dhuey, A. Goltsov, I. Ivonin, E.-B. Kley, C. Peroz, H. Schmidt, and V. Yankov, "Digital optical spectrometer-on-chip," *Appl. Phys. Lett.*, vol. 95, no. 4, pp. 041105-1–041105-3, Jul. 2009.
[27] S. Babin, C. Peroz, A. Bugrov, A. Goltsov, I. Ivonin, V. Yankov, S. Dhuey, S. Cabrini, E.-B. Kley, and H. Schmidt, "Fabrication of novel digital optical spectrometer on chip," *J. Vac. Sci. Technol. B*, vol. 27, no. 6, pp. 3187–3191, Nov. 2009.